ЖЭТФ, 2003, том 124, вып. 5 (11), стр. 1058–1067 © 2003

IGNITION THRESHOLDS FOR DEUTERIUM–TRITIUM MIXTURES CONTAMINATED BY HIGH-Z MATERIAL IN CONE-FOCUSED FAST IGNITION

A. Caruso[*], *C. Strangio*

CR ENEA Frascati, Frascati, RM, Italy

Submitted 6 June 2003

Evaluations of the energy for thermonuclear ignition of a compressed deuterium–tritium mixture contaminated by a high-Z material are presented. Mixing at the atomic level is considered and the results are given as a function of the contaminant fraction. The reference situation is that of cone-focused fast ignition (CFFI). Numerical $2D$ simulations for this study were performed by a Lagrangian $2D$ hydrocode that includes real matter EoS, real matter opacity coefficients, and packages for finite-range energy deposition by reaction products and the relative in-flight reactions. A simple estimate is presented for the effects of high-Z material blobs on the ignition energy (macroscopic mixing). Possible sources for fuel contamination in CFFI are discussed.

PACS: 52.57.-z, 52.57.Kk, 52.57.Fg

1. INTRODUCTION

Thermonuclear ignition thresholds for a compressed deuterium–tritium mixture contaminated by a high-Z material at the atomic level were evaluated as functions of the contaminant fraction. A short pulse of protons was used to start the ignition of a cylindrical assembly of compressed fuel uniformly contaminated by gold at the atomic level. As a reference, a study of the ignition of a clean target at different proton energies was first performed and, after this, the ignition conditions for contaminated targets were found for the selected proton energy. Protons with the proper energy can be used to mock-up deposition by fast electrons such that a part of the study can also be considered useful in predicting the performances for this energy vector.

The $2D$ code COBRAN was used to perform the study. COBRAN includes a «real matter» equation of state and opacity coefficients. The package for driving energy deposition includes light/heavy charged particles, ray-traced laser light, and ray- traced X-rays. The thermonuclear reaction treatment includes finite-range charged particle diffusion and nonthermal nuclear reactions. The diffusion and energy deposition of neutrons is treated by a Monte Carlo code. However, in the cases considered here, the effect of neutrons was marginal and this part of the code was normally not activated [1].

A simple estimate for the effects of high-Z material blobs on the ignition energy (macroscopic mixing) are presented below. The estimate is given in terms of the «cool» surface of the high-Z blobs.

This study can be relevant for the so-called cone-focused fast ignition (CFFI) [2, 3] because in experiments performed for this scheme, the imploded material was found to be contaminated by the cone high-Z material [3, 4]. In the CFFI, a shell containing a layer of DT fuel is actually imploded by soft X-rays or laser light induced ablation, sliding along the external surface of a cone composed by the high-Z material (see Fig. 1*a*). As a result of the implosion, a blob of compressed fuel is formed near the cone tip (see Fig. 1*b*). At this time, a short laser pulse is focused inside the cone to produce a forward jet of fast electrons. Passing through the cone material, the electrons can create an ignition spark on the compressed fuel assembly located nearby. Alternative energy vectors can be the light ions (e.g., protons) produced either by using the fast electrons as a virtual cathode with respect to a properly composed cone tip [3] or by exploding a low-Z foil set in place of the cone terminal portion [1, 5].

High-Z contamination was found in experiments

[*]E-mail: caruso@frascati.enea.it

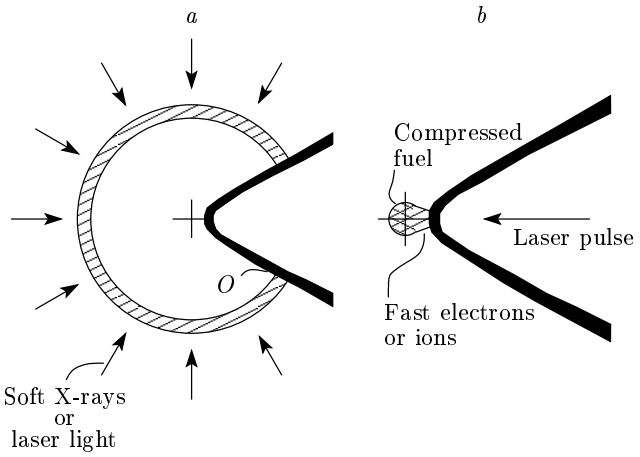

Fig. 1. The cone-focused fast ignition scheme. *a* — Ablation pressure induced by X-rays or laser implodes a fuel shell to form a compressed fuel assembly near the tip of the cone. *b* — A short laser pulse is used to ignite the fuel by fast electrons or energetic light ions

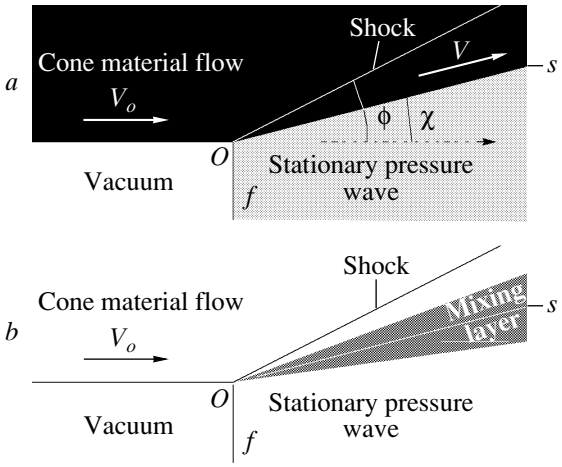

Fig. 2. *a* — The hydrodynamical flow induced in the cone material (black) by the pressure of the imploding shell (gray). *b* — Instabilities at the slip surface s mix cone and shell materials

performed in the indirect drive mode. Vaporization of the cone material (gold) by X-rays (m-lines) passing through the imploding shell was indicated as responsible for this effect [4]. Such a source of contamination should be absent in the direct-drive mode. But another source, potentially also active in this case, can be excited by the onset of the Kelvin–Helmholtz instability on the sliding interface between the imploding shell and the cone surface. We have studied this transient process and found the shell transit near the cone tip to be the most critical stage.

During the implosion, the pressure in the acceleration stage can range from 1 to 100 Mb on the shell and from 1000 to 2000 Mb within the shell material at the transit near the cone tip. Pressures of this order are also exerted on the interface between the shell and the cone material. At such values of pressure, the cohesion forces in the cone material can be neglected and the shell containment by the cone is inertial. This statement is valid for gold as the cone material because the maximum tensile strength of Au estimated from the vaporization specific energy is of the order 0.14 Mb, see Ref. [6]. A very sketchy representation can be used to infer some of the basic flow features just near the leading shell points sliding on the cone (represented by O in Fig. 1*a*). We consider a reference frame attached to O and assume a locally planar $2D$-flow pattern. In this frame, the cone material impinges from the left at the velocity $\mathbf{V}_0$ ($|\mathbf{V}_0|$ is the implosion speed, see Fig. 2*a*). The region behind the leading edge of the imploding fuel shell is roughly mocked up by a stagnating uniform pressure p-wave starting after a rise-front (f). At f, the pressure passes from 0 to p over a distance assumed negligible. Main features of the flow are an oblique shock wave (angle ϕ) deflecting the cone material velocity by the angle χ, from $\mathbf{V}_0$ to $\mathbf{V}$ [7] and a slip surface (s) between the cone and the shell materials represented by the pressure wave.

Assuming the initial pressure on the impinging cone material negligible and assigning p, $\mathbf{V}_0$, and the initial material (solid-state) density ρ_s, the shock parameters follow from the Hugoniot adiabat

$$\varepsilon(\rho, p) = p\left(\frac{1}{\rho_s} - \frac{1}{\rho}\right)/2,$$

where ε is the internal energy per unit mass [7] ($\varepsilon(\rho_s, 0) = 0$) and ρ is the density behind the shock. With p given, ρ follows. To evaluate $\varepsilon(\rho, p)$, we have taken the equation of state for «real materials» included in the previously mentioned $2D$ code COBRAN. In Fig. 3, the resulting Hugoniot adiabat is shown for Au.

Using mass, momentum, and tangential velocity conservation at the shock, we easily determine the quantities V, $\sin\chi$, and $\sin\phi$ (see Fig. 2) as simple functions of the assigned quantities p, ρ_s, and $\mathbf{V}_0$ and of the density ρ corresponding to p in the Hugoniot adiabat. We define the quantities

$$c_0 = \left(\frac{p}{\rho_s}\right)^{1/2}, \quad \xi = \frac{\rho}{\rho_s}, \quad M = \frac{V_0}{c_0}.$$

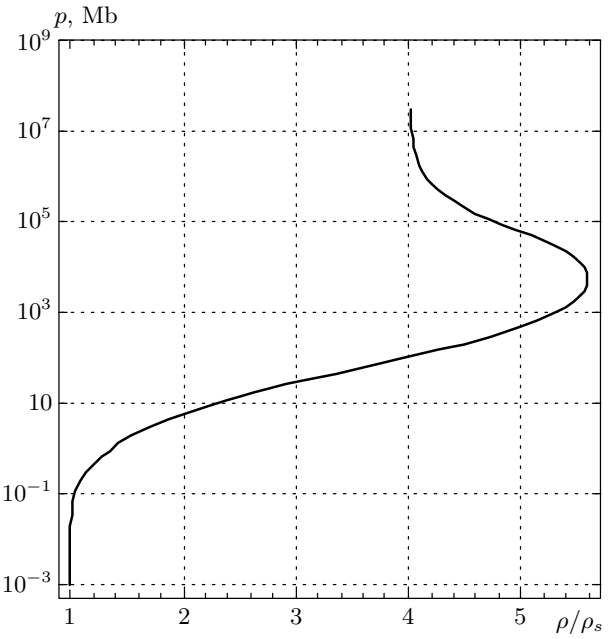

Fig. 3. The Hugoniot adiabat for a shock in gold at the initial solid-state density ρ_s and at the initial pressure set to 0. The adopted equation of state for gold was that on line in the code COBRAN

The oblique shock is formed if

$$V_0 > c_0 \left(\frac{\xi}{\xi - 1}\right)^{1/2}.$$

The relevant quantities for this study are V, χ, and ϕ given by

$$V = V_0 \left(1 - \frac{1 + 1/\xi}{M^2}\right)^{1/2},$$

$$\sin\chi = \frac{1}{M}\left[\frac{\xi - M^2(\xi - 1)}{1 - \xi(M^2 - 1)}\right]^{1/2},$$

$$\sin\phi = \frac{1}{M}\left(\frac{\xi}{\xi - 1}\right)^{1/2}.$$

In Table 1, the above quantities are reported for regimes that can occur in the implosion of a thin spherical shell (e.g., with the in-flight aspect ratio=14). The shell is first set on a low adiabat $\alpha = 0.3$ by a $p_0 = 1$ Mb pressure pulse (the first shock wave, α is the ratio of the thermal electronic pressure to the Fermi pressure). A gradual (adiabatic) rise of the pressure up to $p = 100p_0$ then accelerates the shell to the maximum velocity. The shell material is finally left to freely implode towards the cone tip, where the pressure is expected to be 1000–2000 Mb. The densities $(\rho_{\mathrm{DT}}, \rho_{\mathrm{Au}})$ and the sound velocities $(c_{s\,\mathrm{DT}}, c_{s\,\mathrm{Au}})$ were consistently estimated at the «real matter» level in the flowing cone material (gold) and for $\alpha = 0.3$ in the «DT shell» set at rest. The units are Mb (pressure), g/cm^3 (densities), cm/μs (velocities), and degrees (angles). The effects of the shock wave on the gold flow appear relatively modest in the first two stages of the implosion. Severe flow distortion is produced near the cone tip.

In what follows, we report stability calculations for the slip surface and the corresponding quasilinear evaluation for the mixing layer aperture. Numerical estimates are presented for the cases presented in Table 1.

For any mechanism of fuel poisoning, it is not easy to evaluate the spectrum of sizes/masses of Au finally mixed into the compressed fuel as they undergo a complex evolution before being trapped in the ignition spark area. Two types of contamination can be expected, one in the form of mixing at the atomic level, the other as a distribution of Au blobs in the fuel. For small blobs, a two-step evolution can be expected. In the first, a gold blob immersed in a DT plasma at the temperature 10^8 K or higher and the density $\rho_{\mathrm{DT}} = 200$ g/cm^3 is ablated by electronic thermal conduction and brought to the temperature and pressure equilibrium with the DT fuel. The already mentioned equation of state predicts the density $\rho_{\mathrm{Au}} \approx 435$ g/cm^3 for gold and the average charge $Z_{\mathrm{Au}} \approx 70$. The second step is the diffusion of DT ions through the gold plasma. The diffusion coefficient of the average DT ion through gold plasma is

$$k_{\mathrm{DT}} = \frac{7 \cdot 10^{-14} T_i^{5/2}}{Z_{\mathrm{Au}}^2 \rho_{\mathrm{Au}}}\,\mathrm{CGS}\cdot\mathrm{K},$$

and the diffusion length in a disassembling time is therefore given by

$$R_{crit} = \sqrt{k_{\mathrm{DT}} R_s / c_s}\,,$$

where R_{crit} represents the largest blob that can be diffused through during the spark lifetime. The previous estimate can be set as

$$R_{crit} = \frac{0.003}{\sqrt{\rho_{\mathrm{DT}}\rho_{\mathrm{Au}}}}\ \mathrm{cm}$$

by setting the ion temperature to 10^8 K in the previous formula, $R_s = 0.5/\rho_{\mathrm{DT}}$ cm (as typically required for ignition), and $Z_{\mathrm{Au}} = 70$. The mass corresponding to these values is

$$M_{crit} \approx \rho_{\mathrm{Au}} R_{crit}^3 = \frac{2.7 \cdot 10^{-8}}{\rho_{\mathrm{Au}}^{1/2}\rho_{\mathrm{DT}}^{3/2}}.$$

For $\rho_{\mathrm{Au}} \approx 435$ g/cm^3 and $\rho_{\mathrm{DT}} = 200$ g/cm^3, $R_{crit} \approx 0.1$ μm and $M_{crit} \approx 5 \cdot 10^{-13}$ g.

Table 1.

Reference case	p	V_0	ρ_{DT}	$c_{s\,\mathrm{DT}}$	V	ρ_{Au}	$c_{s\,\mathrm{Au}}$	χ	ϕ
First shock wave	1	6	0.78	1.7	≈ 6	26.2	0.42	1	7.5
End of accelerating pulse	100	15	10	4.3	14.8	76	1.6	7.6	10

Below, we report evaluations for the amount of Au (atomic mixing) or the sizes of blobs (macroscopic mixing) necessary to obtain a relevant effect on the ignition threshold in the two contamination modes.

2. IGNITION STUDIES

The ignition studies for contamination at the atomic level were performed for cylinders of a compressed DT+Au uniform mixture at the initial densities around 200 g/cm^3, irradiated by a proton beam along the axis. Advantages in using light ions for fast ignition were considered in Ref. [8]. At any rate, proton beams with the proper pulse and particle energy can be used to roughly mock-up deposition by fast electrons as both these energy vectors give energy mostly to the electrons in the target.

The length of the cylinder (S) was taken equal to the diameter ($2R$) and set to 300 μm. The intensity distribution of the beam as a function of the radius r was Gaussian, proportional to $\exp(-r^2/R_0^2)$ for $r \le 2R_0$ and 0 outside. The scale R_0 was set to 25 μm. The pulse duration was taken 15 ps, short enough to make the expansion negligible during irradiation. The time dependence was a linear ramp for the first 5 ps and constant for the remaining 10 ps.

The initial fuel composition was assigned by giving the numeric fractions

$$f_{\mathrm{Au}} = \frac{n_{\mathrm{Au}}}{n_{\mathrm{Au}} + n_{\mathrm{D}} + n_{\mathrm{T}}}, \quad f_{\mathrm{D}} = f_{\mathrm{T}}, \quad f_{\mathrm{Au}} + f_{\mathrm{D}} + f_{\mathrm{T}} = 1,$$

where n_{Au}, n_{D}, and n_{T} are the numeric densities of gold, deuterium, and tritium. In the simulations, $n_{\mathrm{D}} = n_{\mathrm{T}}$ was initially assigned.

The initial target density was either set equal to 200 g/cm^3 or adjusted for each value of f_{Au} such that the total pressure (p) is equal to that of a clean reference target at 200 g/cm^3 and $\alpha = 0.3$, assuming uniform temperature. The second case was considered to simulate equilibrium between the contaminated region where the ignition spark is formed and a contiguous clean fuel at the specifed reference conditions. For our «real matter» equation of state, this implies that ρ increases with f_{Au}.

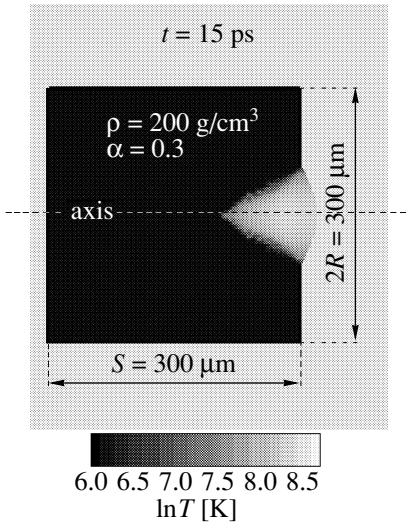

Fig. 4. Electron temperature distribution in a pure DT cylindrical target at the end of the igniting proton pulse (pulse energy 40 kJ, proton energy 1 MeV)

In Fig. 4, we show the electron temperature distribution in a clean reference target ($f_{\mathrm{Au}} = 0$, $\rho = 200$ g/cm^3) at the end of a 40 kJ, 1 MeV igniting proton pulse.

2.1. Ignition of a clean fuel

The ignition energy (E_{ign}) for a clean fuel at $\rho = 200$ g/cm^3 is represented in Fig. 5 as a function of the ion (proton) kinetic energy (E_{kin}). No ignition occurs at less than 40 kJ. The total fusion energy released by the target after complete disassembling is about 540 MJ, the radiated energy is about 5 MJ, and the fractional burn-up is $f_b = 0.38$.

The ignition of a compressed clean fuel by light ions presents several typical features. One, clearly seen in Fig. 4, is the rather spiked structure of the spark in spite of the smooth Gaussian space distribution of the irradiation. This feature is simply explained by noting that the range of the ions increases with temperature and this depends on the amount of energy deposited. The ion range is therefore a self-consistent fea-

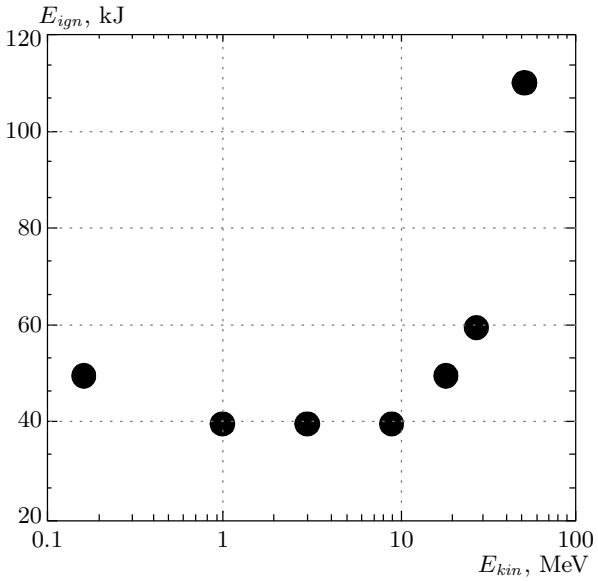

Fig. 5. Ignition energy for a 200 g/cm^3 DT fuel by a proton beam as a function of the proton kinetic energy

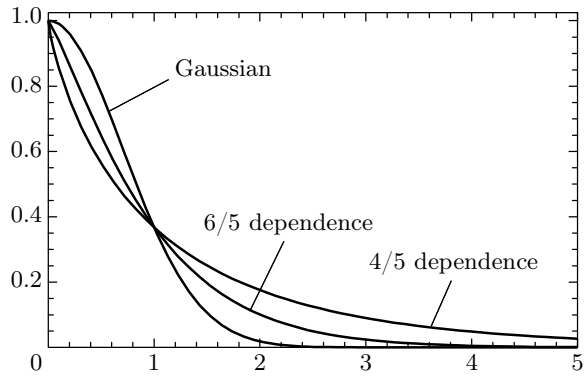

Fig. 6. Space distributions for ρL, T_e, and E_s according to Eqs. (2a) and (2b)

ture. During the irradiation, a bleaching wave is formed allowing a deeper ion penetration into the target in the regions where the temperature is higher, namely near the ion beam axis. Neglecting thermal diffusion, nuclear heating, and «cold» target range, this effect can be estimated as follows:
for the range (L) equation

$$\rho L \propto E_{kin}^{1/2} T_e^{3/2}, \tag{1a}$$

and for the energy equation

$$\rho L T_e \propto E_s(r,t), \tag{1b}$$

where $E_s(r,t)$ is the energy deposited per unit surface. These equations imply that

$$T_e \propto E_{kin}^{-1/5} E_s^{2/5}(r,t) \propto E_{kin}^{-1/5} \times \exp\left[-\left(\frac{r}{R_0}\right)^{4/5}\right], \tag{2a}$$

$$\rho L \propto E_{kin}^{1/5} E_s^{3/5}(r,t) \propto E_{kin}^{1/5} \exp\left[-\left(\frac{r}{R_0}\right)^{6/5}\right]. \tag{2b}$$

The different dependences are represented in Fig. 6. The spiked structure is clearly shown for both ρL and T_e.

Peculiar structures and behaviors can be detected in burn waves. In Fig. 7, we show the development and propagation of the burn wave for a target irradiated by a 40 kJ, 1 MeV beam of protons. Up to 80 ps, burn propagation occurs through a mode featured by in-cavity burning and alpha-particle ablation driven shock front. The shock generated by ablation pressure rises the density up to approximately 570 g/cm^3. In the ablation front, the density drops to about 36 g/cm^3 over a distance of about 40 μm. Near $t = 80$ ps, a new propagation mode starts. A quasispherical shock wave detaches from the tip of the ablation front and burning propagates as a detonation wave starting from a point near the initial fuel assembly center. The produced thermonuclear power W_{Tn} and energies are also shown in Fig. 7; we note the bell-like time dependence of the power. Density profiles along the cylinder axis z are shown in Fig. 8 for two propagation modes.

The burn propagation pattern can change substantially if the igniting pulse energy is well above the threshold. This can be seen in Fig. 9, where the density maps are represented in the case where the energy of the igniting pulse rises from 40 kJ to 70 kJ, with the other parameters unchanged. After a fast radial propagation, the detonation propagates along the target axis. The thermonuclear energy power release presents a plateau corresponding to the propagation along the cylinder axis.

Highly structured detonation waves can also be found. In Fig. 10, a 27 MeV beam of protons starts ignition at 60 kJ. Both the radial wave and tip starting waves propagate and ultimately coalesce in a single wave propagating along the axis.

2.2. Ignition of a fuel contaminated by high-Z materials (Au)

In this section, we present the results of simulations performed to study fast ignition thresholds of a fuel uniformly doped by gold. Studies of the effects of light impurities (C, Si, and O) on the performances of directly driven targets were published in the past [9].

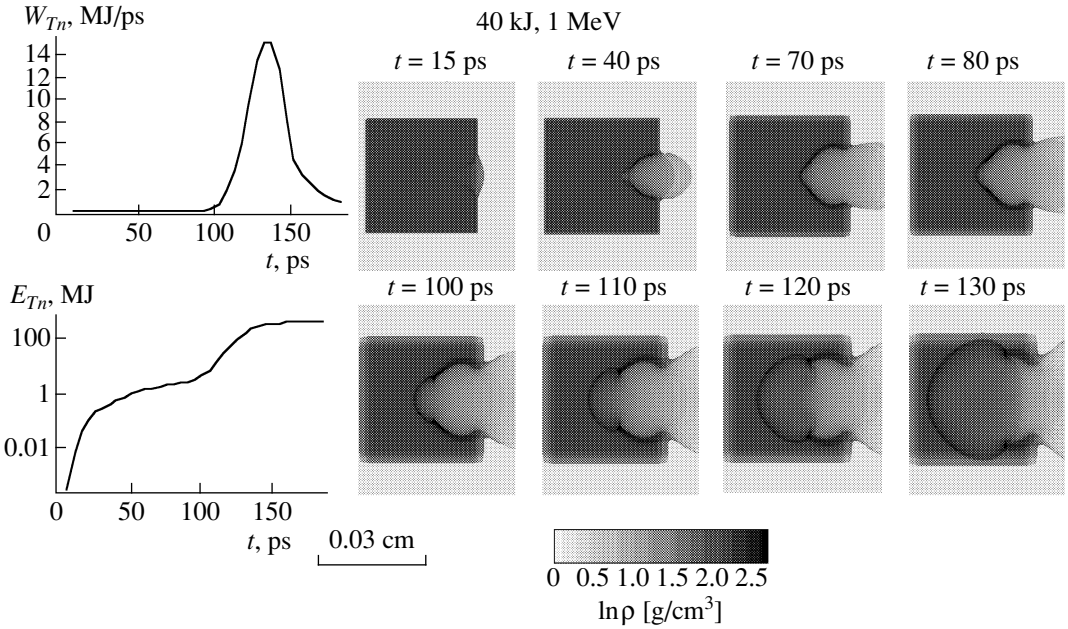

Fig. 7. Burn propagation for the ignition spark shown in Fig. 1. Density maps. The propagation for the lowest energy needed to ignite the considered fuel assembly is represented. After propagation in the α-particle ablation driven mode, a detonation wave is started near the initial fuel assembly center, at the tip of the ablation front. The produced thermonuclear (Tn) power and energies are also shown; we note the bell-like time dependence of the power

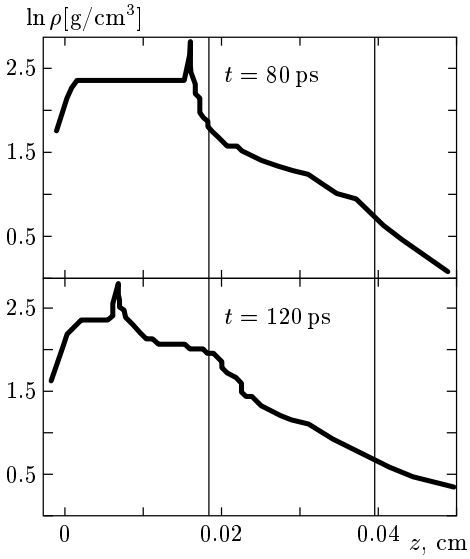

Fig. 8. Density profile along the cylinder axis at different times showing features of the two burn propagation modes

In the investigations for $f_{\mathrm{Au}} \neq 0$, the energy E_{kin} was set to 1 MeV (corresponding to the ignition energy $E_{ign} = 40$ kJ for the clean case, see Fig. 5) and f_{Au} was increased from 0.001 % to 1.5 %. The introduction of high-Z contamination affects the ignition thresholds through several mechanisms. Some of these are detectable through inspection of Fig. 11. The electron temperature maps are given at the end of the igniting pulse for different degrees of doping. It can be seen that by increasing f_{Au}, the needed electron temperature increases. At the largest doping, the spark is imbedded in a thick radiation wave. The presence of gold affects the heat capacity and through this the igniting beam penetration depth, which is a self-consistent feature. The spiked structure disappears. The difference between T_e and T_i increases with f_{Au}. The situation evolves very rapidly, however. Actually, 10 ps later, for $f_{\mathrm{Au}} = 1$ % for instance, due to diffusive losses and relaxation effects, the electron temperature decreases to 26 keV and the maximum ion temperature achieves the value of approximately 39 keV. In this same case, the simulations show that due to the reduced DT content (about 57 %) and to a smaller fractional fuel burn-up (about 25 % instead of 38 % of the clean fuel), the yield is decreased to about 40 % that of the clean fuel case. It is important to remark, however, that the calculations presented here are relevant to assess whether ignition occurs for a given contamination of the spark region. The previous considerations relative to the yield can be

taken as meaningful in the case where contamination is truly uniform.

The results of the investigation for $f_{\mathrm{Au}} \neq 0$ are shown in Fig. 12, where the data for the assigned density or pressure are shown. The two fitting curves are similar (exponential functions), with the one for a constant pressure (circles) being somewhat shifted to the right. In both cases, E_{ign} presents a steep increase as f_{Au} approaches 0.2 % (about 14 % by mass). For greater values of f_{Au}, the increase in E_{ign} is very fast.

3. EFFECTS OF MACROSCOPIC CONTAMINATION

With regard to the effects of macroscopic mixing, we estimate the typical size of the blobs that have a substantial effect on the ignition thresholds. Assuming the surface of a contaminant blob to be a sink for the fuel energy through the electron thermal flow, we can estimate the order of magnitude of the power W_a absorbed in the ignition spark by the contaminant as

$$W_a \approx \kappa_e T_e^{7/2} 4\pi \sum R_b.$$

Here, κ_e is the Spitzer thermal conductivity coefficient and $\sum R_b$ is the sum of the blob radii contained in the spark. The total energy absorbed before spark disassembling is

$$E_a \approx W_a (R_s/c_{s\,\mathrm{DT}});$$

this value has to be compared with the spark thermal energy E_{th}. For a standard spark ($T \approx 10$ keV, $\rho_{\mathrm{DT}} R_s \approx 0.5$ g/cm^2), we find that

$$\frac{E_a}{E_{th}} \approx \frac{3.8 \sum R_b}{R_s}.$$

Setting this ratio to 0.5 implies that

$$\sum R_b \approx 0.13 R_s.$$

4. THE KELVIN–HELMHOLTZ INSTABILITY AT THE SHELL–CONE INTERFACE

In the reference cases in Table 1, a treatment of the Kelvin–Helmholtz instability for compressible fluids with a discontinuous density and velocity of sound was required. The adopted geometry is shown in Fig. 13. The plane xy is taken on the slip surface s and the wave number is taken in the plane xz. The flow is assumed at rest for $z < 0$, in the region occupied by the imploding shell material. In the $z > 0$ region, where the cone material flows, the velocity is set to the velocity V resulting from the shock analysis. Assuming that the perturbed quantities behave as $\exp[-i\omega t + i(k_x x + k_z z)]$, we write the dispersion relation

$$c^2 r^2 (\nu^2 \omega^2 - 4)(\omega - 2)^4 - \left[\nu^2 (\omega - 2)^2 - 4c^2\right] = 0, \quad (3)$$

where

$$r = \frac{\rho_{\mathrm{Au}}}{\rho_{\mathrm{DT}}}, \quad c = \frac{c_{s\,\mathrm{Au}}}{c_{s\,\mathrm{DT}}}, \quad \nu = V \frac{\cos\psi}{c_{s\,\mathrm{DT}}},$$

and the complex frequency ω is normalized by $k_x V \cos\psi/2$. The study was performed numerically and the results are as follows. The interface is always unstable for waves with $90^\circ \leq \psi \leq \psi_2$, where $\psi_2 \geq 0$. In this interval, the growth rate γ (the imaginary part of ω) starts from 0 at $\psi = 90^\circ$, achieves a maximum γ_m at some ψ_m, and vanishes again for $\psi = \psi_2$ if $\psi_2 > 0$. Furthermore, unstable modes can be found when $\gamma \neq 0$ for $\psi_2 = 0$. All these unstable modes correspond either to a reduced component of the velocity V along x ($\psi_2 > 0$) or to a sufficiently small value of V itself (for $\psi_2 = 0$ and $\gamma \neq 0$). It is therefore possible to say that for these modes, the fluids behave as incompressible. The results obtained in the reference cases are reported in Table 2, where ψ_m and ψ_2 are expressed in degrees,

$$\gamma_0 = \frac{\gamma_m}{k_x c_{s\,\mathrm{DT}}}, \quad \tau = \frac{\Delta}{\gamma_m t_{transit} \lambda_x},$$

Δ is the shell thickness, $t_{transil} = \Delta/V_0$, and $\lambda_x = 2\pi/k_x$. When $\tau(\lambda_x/\Delta) < 1$, the instability arises.

In conclusion, the slip surface is always unstable. The maximum growth rate is found in the regime near the tip cone, where all perturbations with $0^\circ \leq \psi < 90^\circ$ are unstable. The formation of mixing layers like that represented in Fig. 2*b* can be expected over most of the implosion process.

Semiempiric theory [10] and numerical simulations [11, 12] have been used in the description of mixing layers. Quoted in Ref. [10] are experiments and theories for turbulent mixing in the case of large differences in density or supersonic flows. Difference in density seems to slightly affect the width of the mixing layer (the half width h), whereas this becomes somewhat narrower for supersonic flows.

In what follows, we adopt a tentative dimensional model to estimate h in the reference cases. We assume that

$$h^2 \approx D(x/V), \quad D = a\gamma_m h^2,$$

a is a suitable number, x is the distance from O along $\mathbf{V}$ (see Fig. 2*b*), and γ_m is evaluated for a typical wave number $k_x \approx h^{-1}$. Because

$$\gamma_m \propto h^{-1},$$

we find that

$$h \propto x.$$

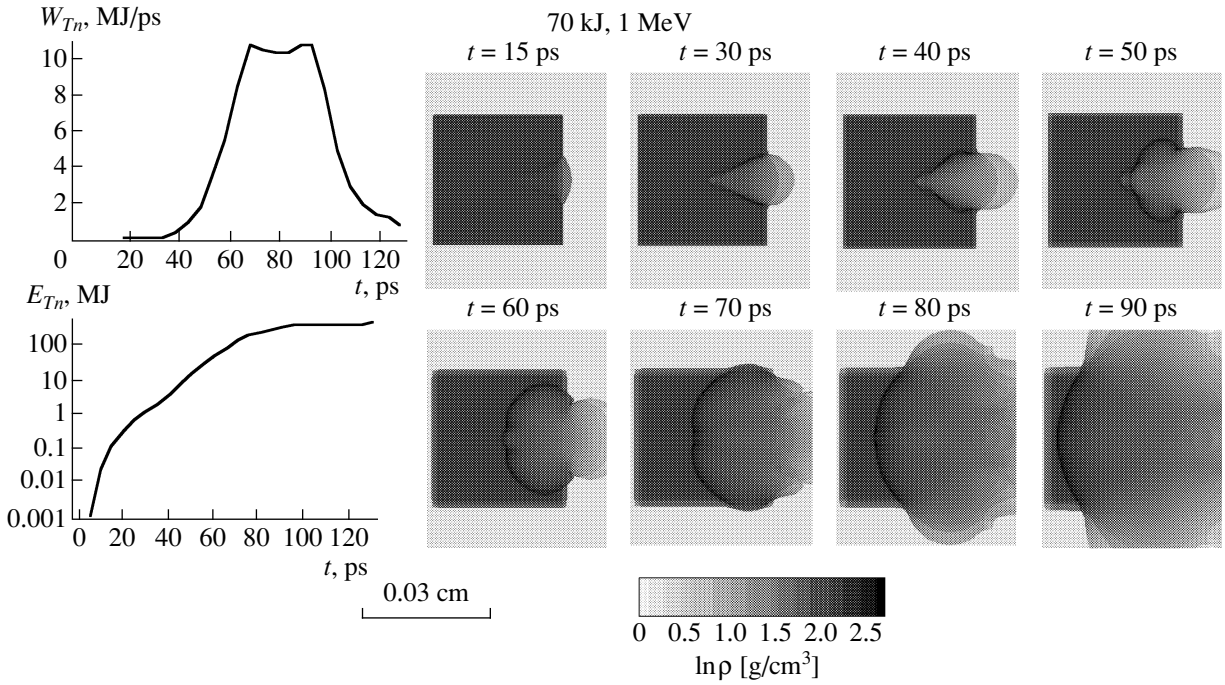

Fig. 9. Burn propagation through a target irradiated by an energy pulse well above the threshold. The detonation propagates first in the radial direction and then along the axis. The plateau on the burn rate curve (to be compared with the bell-like shape shown in Fig. 7) is connected to the axial propagation

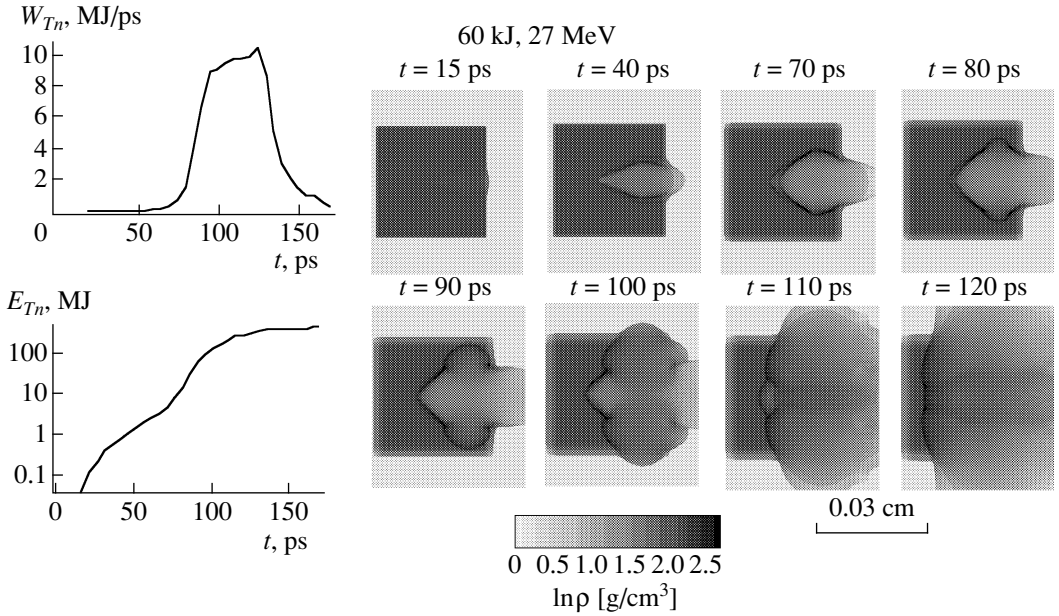

Fig. 10. Burn propagation for a target ignited by a 27 MeV proton beam. Density maps. The burn wave is highly structured. This results from simultaneous propagation of waves in the radial direction and from the heated zone tip. The situation is a hybrid of the cases shown in Figs. 5 and 7

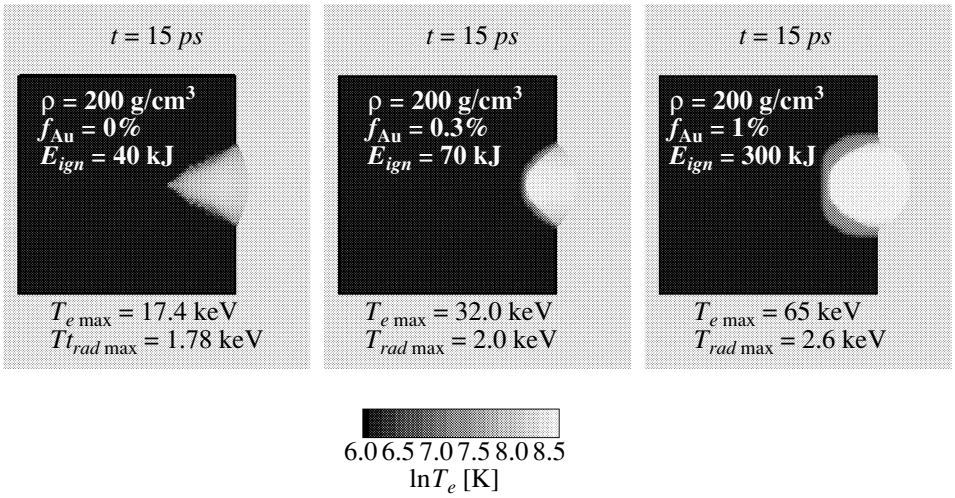

Fig. 11. Comparison between the electron temperature distribution maps for increasing f_{Au} at the end of the proton beam irradiation. We note the change in the spark shape. The thick gray feature for $f_{\mathrm{Au}} = 1\,\%$ is due to radiation pre-heating and the maximum radiation temperature increases with f_{Au}. The same trend occurs for the difference of temperature between electrons and ions. This, however, is a highly transient situation: 10 ps later, for $f_{\mathrm{Au}} = 1\,\%$ for instance, due to diffusive losses and relaxation effects, the electron temperature decreases to 26 keV and the maximum ion temperature achieves the value about 39 keV

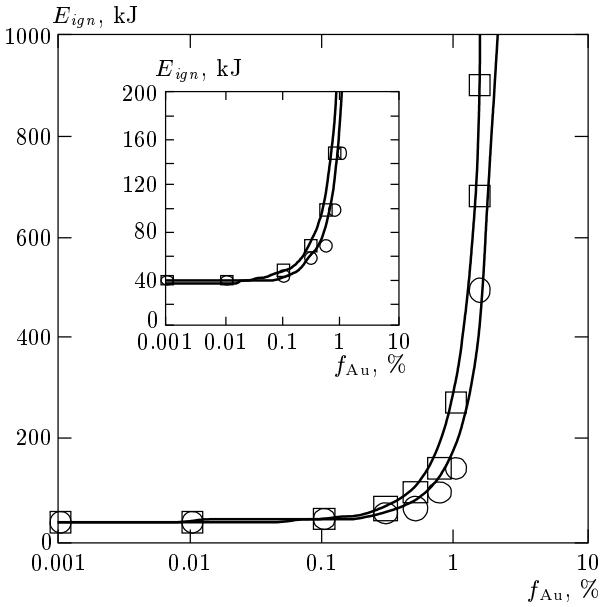

Fig. 12. The ignition energy for 1 MeV protons represented as a function of the Au doping. Squares refer to the fuel at the assigned density ($\rho = \mathrm{const} = 200$ g/cm^3) and circles refer to the fuel at the assigned pressure ($p = \mathrm{const}$). In both cases, the ignition threshold presents a steep increase as f_{Au} approaches 0.2 % (see a magnification in the insert). The fitting curves are exponential

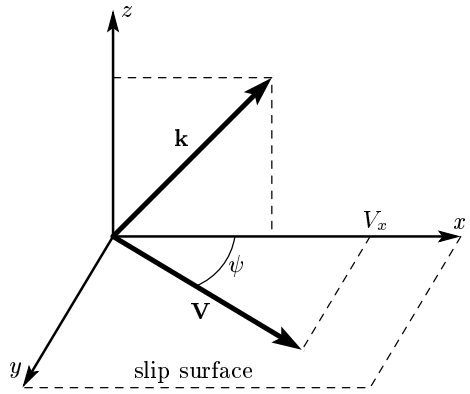

Fig. 13. Geometry for the Kelvin–Helmholtz instability calculations

Table 2.

Reference case	ψ_m	ψ_2	γ_0	τ
First shock wave	86	70	0.046	10
End of accelerating pulse	82	73	0.11	5

For $a \approx 0.2$, the previous model applied to incompressible flows with a uniform density agrees with the experiment [10]. In the cases considered here, the angle $\theta_{mix} = 2h/x$ is

$$\theta_{mix} = 2a\gamma_0 c_{s\,\mathrm{DT}}/V.$$

The maximum thickness of the mixing layer is

$$\delta_{mix} \approx \theta_{mix}\Delta;$$

in the previously assumed reference situations, the results, ordered for increasing pressure, are $\theta_{mix} \approx 5, 10$, and 70 mrad, and hence, for $\Delta = 100$ μm, we have $\delta_{mix} = 0.5, 1$, and 7 μm.

It seems safe to conclude that at the sliding surface, the Kelvin–Helmholtz instability, which is active during the shell implosion, is especially effective in the «near tip» region where a substantial amount of matter can be collected and mixed into the fuel. An indication for this can be found by the following considerations.

Typically, the fuel masses of interest in CFFI (M_f) are of the order 3 mg at a density about 200 g/cm^3. The typical spark masses (M_{spark}) are of the order 3 μg. The quantities M_f and M_{spark} are to be compared with that of gold (M_{Au}) involved in the mixing. Estimating the thickness of the mixing zone as $\delta_{mix} \approx \theta_{mix}\Delta$, the volume involved in mixing by a shell sweeping the cone surface by a length L along the cone up to the cone apex is

$$V_{mix} = \pi \sin\theta L^2 \delta_{mix},$$

where θ is the cone half aperture. The amount of gold involved in mixing can be estimated as $0.5\rho_{\mathrm{Au}}V_{mix}$ and assuming that a fraction f is entrained to the fuel, it is found that

$$M_{\mathrm{Au}} = 0.5\rho_{\mathrm{Au}}V_{mix}f.$$

If this estimate is applied to the «near tip» case for a cone with $\theta = 30^\circ$, at $L = 400$ μm and $f = 0.3$, it follows that $M_{\mathrm{Au}} \approx 30$ μg or $M_{\mathrm{Au}} \approx 10M_{spark}$. In the ignition study, it was found that a 14 % mass contamination was sufficient to make ignition practically impossible. Under the previous conditions, this critical situation can be created on a mass about 30 times the spark mass. Clearly, the relevance of Kelvin–Helmholtz instability can be completely assessed only after using a more complete description that would include the final space distribution of the contaminant. However, the previous estimate indicates that substantial amounts of contaminant can be potentially involved in the process.

5. CONCLUSIONS

The process of fast ignition by light ions has been studied and the ignition thresholds for different ion kinetic energies have been found for the fuel composed by 50 % deuterium and 50 % tritium. The self-consistent structure of the igniting spark has also been determined by analytic methods. The physics of the burn propagation has been studied in some detail as a function of the irradiation parameters. Because the cone material can contaminate the fuel in cone-focused fast ignition, a parametric study has been performed to find how the ignition thresholds depend on the level of contamination. This study, performed for an atomically mixed contaminant, has shown that the level of atomic contamination about 0.2 % by number is sufficient to render ignition practically impossible.

Evaluations have also been performed to find the possible effects on ignition of contaminant blobs mixed to pure DT fuel.

Finally, it has been shown that in addition to cone vaporization due to X-rays passing through the imploding shell in the indirect drive mode, another source of contamination can be a turbulent mixing at the interface cone-imploding shell. This mechanism could also be active for directly driven implosions.

We are grateful to N. V. Zmitrenko (IMM, Russian Academy of Sciences) for very useful discussions on the Kelvin–Helmholtz instability.

REFERENCES

1. A. Caruso and C. Strangio, Laser and Part. Beams **19**, 295 (2001).
2. R. Kodama et al., Nature **412**, 798 (2001).
3. S. Hatchett et al., in *Proc. of 43rd Meeting Division of Plasma Physics*, APS (2001).
4. R. B. Stephens et al., Preprint GA-A24140 (2002).
5. A. Caruso and R. Gratton, Phys. Lett. A **36**, 275 (1971).
6. Ya. B. Zel'dovich and Yu. P. Raizer, *Physics of Shock Waves and High-Temperature Hydrodynamic Phenomena*, Academic Press (1966).
7. L. D. Landau and E. M. Lifshitz, *Theoretical Physics, Vol. VI, Hydrodynamics*, Nauka Publishing, Moscow (1988).
8. M. Roth et al., Phys. Rev. Lett. **86**, 436 (2001).
9. R. A. Sacks and D. H. Darling, Nucl. Fusion **27**, 447 (1987).
10. H. Schlichting, *Boundary Layer Theory*, McGraw-Hill (1968).
11. V. A. Andronov et al., Preprint LA-12896 (1995).
12. M. Lesieur, *Turbulence in Fluids*, Kluwer Academic Publishers (1990).